Contribution of the thermal inertia of trains to the primary frequency control of electric power systems

Jesús Araúz, Sergio Martínez

Contribution of the thermal inertia of trains to the primary frequency control of electric power systems

Jesús Araúz[a,b,c*]; Sergio Martinez[a]

[a]*Escuela Técnica Superior de Ingenieros Industriales, Universidad Politécnica de Madrid, C/José Gutíerrez Abascal, 2, 28006, Madrid, Spain*
[b]*Panama Railway Engineering Research Group, Faculty of Electrical Engineering, Universidad Tecnológica de Panamá, Panama City, 0819-07289, Republic of Panama*
[c]*Research group Energy and Comfort in Bioclimatic Buildings, Faculty of Mechanical Engineering, Universidad Tecnológica de Panamá, Panama City, 0819-07289, Republic of Panama*

Abstract

There is a wide consensus about substituting fossil fuel-based electric generation with renewable resource-based one. However, the displacement of conventional power plants with power electronics-interfaced plants implies several technical issues that must be addressed. Among these needs, providing ancillary services to electric power systems is fundamental to maintain power quality and system reliability. There is a considerable amount of literature about providing ancillary services from renewable power plants and an increasingly important effort to complement these services with loads. However, the contribution of railway systems to these services has been less explored. Considering the world-wide expansion of railway systems, it is appropriate to consider them as relevant contributors to ancillary services. The present work presents a novel approach to assess the possibilities of contribution of railways to grid primary frequency control based on the thermal inertia of trains. This approach aims at determining how railways can support frequency control tasks without affecting the circulation time of trains and thermal comfort of passengers. This paper proposes to act on the power consumption of the air conditioning system of trains as the way of making the train whole consumption responsive to frequency deviations. In addition, the paper proposes a methodology for analyzing the effectivity of the approach. It defines the extent of the modeling detail of railway and electric power system, and the coupling between them. To validate the feasibility, its application is illustrated with a case study. The results show that frequency deviations can be reduced without affecting passengers' thermal comfort.

Keywords: frequency control, thermal inertia, railway, demand response

1. Introduction

Due to the current worldwide energetic transition, renewable energy-based power plants are increasing their presence in electric power systems. This growing is towards the reduction of the usage of fossil-based energetic resources and the mitigation of adverse effects on environment [1]. Contrary to conventional power plants, the renewable energy-based power plants do not intrinsically have the capacity to provide ancillary services as: response under fault, frequency-power control, reactive power-voltage regulation, etc. Therefore, if these novel power plants displace a considerable amount of conventional plants, the rest of the actors of electric power systems (not only generators but also consumers) must modify their conventional behavior so as to cooperate in providing safety, reliability, and power supply quality [2].

Many researchers have investigated how to face these problems. For example, without the aim of being comprehensive: Ochoa *et al*. [3], [4] provided modeling and control methods for wind power plants to support the

primary frequency control by means of modifying the maximum power point tracking curve and the pitch angle; Golieva [5] assessed the connection of wind farms to weak public grids; Julien *et al.* [6] presented a hierarchical control system for photovoltaic plants to provide ancillary services to grid and to mitigate the generation variability; Pierro *et al.* [7] proposed a flexible photovoltaic plant structure, for the mitigation of system imbalance, based on proactive power curtailment and storage fully managed as secondary reserve; Kryonidis *et al.* [8] reviewed the most important ancillary services (voltage regulation, voltage unbalance mitigation, congestion management, power smoothing, reactive power support, inertial response, and frequency response) for future application into distribution and transmission networks; and Tamrakar *et al.* [9] reviewed the role of virtual inertia, considering different approaches and applications.

Apart from recognizing the complexity of maintaining stability in power systems, the integration of new market mechanisms and grid codes is needed to seize the possible benefits [10]. Many reviews on actual regulation framework have been done. Some, as Carroll *et al.* [11], are focused on assessing the current regulations, codes, and standards to anticipate the needs of updating them. Others, as Gokhale-Welch *et al.* [12], attempt to extract the best practices of world-wide codes to address a technological challenge in a region which lacks appropriate codes.

In Literature, there are many published works on the integration of renewable energy-based power plants in the grid. On the other hand, due to the current technological development on communication and control techniques, consumers can also participate in grid support tasks by adjusting their consumption behavior. This is generally known as "demand response", which can be based on the response to different signals (energy prices, incentives, or physical magnitudes, among others) [13]. Similarly to optimization programs applied to power plants, it is also possible to optimize the demand behavior as function of energy costs/prices, peak hours, pollution, technical restrictions in electric grids, preferences of consumers, etc. [14]. Hence, the demand response integration must include a deep analysis of load requirements, grid operational limits, and even the interaction with other energy systems as heat and/or fuel hubs, microgrids, islanded grids, etc. [15].

It is possible to find several recent works on demand response. Among others, Yumiki *et al.* [16] developed an autonomous Vehicle-to-Grid (V2G) for providing primary frequency control and voltage amplitude regulation to transmission and distribution grids, respectively, from onboard batteries. Ledro *et al.* [17] studied the contribution of electric vehicle fleets, seen as virtual power plants, to compensate the power fluctuations induced by wind-based generation. Blatiak *et al.* [18] proposed a framework for optimal trip scheduling of electric vehicle fleets based on mixed-integer linear algebra. Also, the quantifying of potential profits for commercial electric vehicle fleets is done. Diaz-Londono *et al.* [19] presented a conceptual framework for network aggregators to contribute to the flexibility required on the generation and demand side. Here, different types of loads are managed according to their capabilities of providing ancillary services but restricted by their dynamics and flexibility.

In summary, those loads with a considerable presence in electric power systems can contribute significantly to the provision of grid ancillary services. According to the International Energy Agency (IEA) [20], the railway sector represents the 1.9% of global energy consumption. This energy amount is smaller than other sectors' due to the current high efficiency in railway technology. Nevertheless, railway demand response has been studied from different perspectives, as distributed generation integration, recovery of regenerative braking energy, microgrids, etc. [21]–[23], the main focus being the energy trading between the railway and the grid.

There are few works about railway demand response for grid supporting tasks, and even less about contributing to grid frequency control. For example, He *et al.* [24] proposed a novel frequency regulation framework based on day-ahead capacity estimation, real-time response, and frequency control parameters dispatch. To satisfy the frequency control requirement, and a multi-train response strategy, a novel sequential cutting plane algorithm was developed to coordinate individual train dynamics and solving optimally the capacity estimation and power dispatch problems. By means of numerical studies, He *et al.* [24] verified the effectivity of the proposed framework and concluded about the high potential of supporting frequency control. However, the application of this approach requires the use of optimization methods, large differential equation constraints, considerable computational resources, etc. Moreover,

the proposed frequency regulation framework demands the modification of the running processes of trains. Hence, although the average circulation time can be achieved by compensating decelerations with accelerations, and reciprocally, the dwelling and arrival times can be affected, as well as other mechanical considerations.

In the present work, we propose an alternative method for the railway to contribute to grid primary frequency control without affecting the circulation time of trains. It is based on the variation of the electric power consumption of the air conditioning system of trains in response to grid frequency variations. This consumption variation modifies the instantaneous load seen by the grid and, therefore, can contribute to primary frequency control. As thermal dynamics of trains are much slower than grid primary frequency dynamics, this can be done with a low affection to thermal comfort of passengers. Apart from reducing grid frequency fluctuations due to non-railway events, the proposed approach can be also used to minimize the adverse effects of certain train operations on grid frequency. To the best of our knowledge, this is the first time railway HVAC systems are considered to contribute to grid frequency control. The main contribution of the present work is the novel way of providing support to grid frequency control tasks from railways without risking the effectiveness of passenger transport. This relies on the coupling between the railway thermal performance, and its electrical interaction with the grid.

To validate the feasibility of the proposed approach and to explore its possibilities, we present a case study and the behavior of electrical and thermal magnitudes facing different situations. Section 2 of the paper describes models of the railway system, the electric power system, and their coupling. Section 3 presents the case study and Section 4 the analyzed situations. Section 5 draws the main conclusions.

2. Methodology

Changing the operation of heating, ventilation, and air conditioning (HVAC) systems as a way of demand response from office and commercial buildings has been extensively studied, for example [25]. The thermal modeling of buildings, which includes the envelope characterization and analysis of heat fluxes, is mandatory for an appropriate building demand response [26], [27]. Similarly, in the case of railway systems, apart from the electrical and dynamic modeling of the rolling stock, railway layout, and catenary, a thermodynamical modeling of trains is needed. On the other hand, since the study is oriented to grid frequency control, the power system modeling must be based on frequency related parameters, as the damping of load, rotative equivalent generator mass, speed regulator topologies, etc.

2.1. Railways

Railway models have been extensively developed [28]–[34], where the model accuracy varies according to the study scope. For the type of assessment proposed in the present work, the calculation of the individual power consumption of a train is needed, specifically including auxiliary power consumption (P_{Aux}). The train power is described in equation (1), where: $m\ a$ represents the product between the mass and the acceleration of the train, F_{mec} stands for the mechanical resistance forces, v is the instantaneous train speed, η_{total} is the global efficiency, and P_{Aux} represents the auxiliary consumption, as communication services, lighting, HVAC system, etc.

$$P_{elect\ total} = \frac{(m\ a + F_{mec})\ v}{\eta_{total}} + P_{Aux} \tag{1}$$

F_{mec} is the sum of all the resistances based on aerodynamics (F_{aero}), slope (F_{slope}), radius of curvature (F_{curve}), and tunnels (F_{tunnel}). Equations (2)-(5) represent their models, respectively. Here, A, B, and C are the Davis equation coefficients for aerodynamic resistance defined by mass, stiffness, and damping, respectively; $m\ g$ represents the product between the train mass and the gravity acceleration; ang_{slope} is the rail layout angle; R is the radius of curvature

of the rail layout; L_{train} is the train length; ang_d is the deflection angle; and L_{tunnel} is the length of the tunnel [35]. Generally, the input data of equations (2)-(5) can be obtained from railway companies, especially those related to track layout (v, ang_{slope}, ang_d, and, R). Davis coefficients and train characteristics are given by manufacturers.

$$F_{aero} = A + B\,v + C\,v^2 \tag{2}$$

$$F_{slope} = m\,g\,\sin(ang_{slope}) \tag{3}$$

$$F_{curve} = \begin{cases} \dfrac{0.6\,m\,g}{R}, & R \le L_{train} \\ \dfrac{0.0105\,m\,g\,(ang_d)}{L_{train}}, & R > L_{train} \end{cases} \tag{4}$$

$$F_{tunnel} = 1.3x10^{-7} m\,g\,L_{tunnel} \tag{5}$$

On the other hand, according to the focus of the present work, the auxiliary power, P_{Aux}, is mainly defined by the power required by the HVAC ($\dot{Q}_{HVAC}$) as shown in equation (6). The heat power delivered by the HVAC system varies depending on: the injected air flow ($\dot{V}$), the air density (ρ), the air specific heat at constant pressure (C_p), and the difference between the train inner air temperature and the injected air temperature (ΔT). As an approximation, the injected air temperature is equal to the HVAC setpoint one. The total electrical auxiliary power can be computed by adding the resulting heat power divided by the average HVAC system efficiency (COP_{mean}) and the rest of the other n auxiliary consumptions (P_i).

$$P_{Aux} = \frac{\dot{Q}_{HVAC}}{\mathrm{COP}_{mean}} + \sum_{i=1}^{n} P_i\,, \qquad \dot{Q}_{HVAC} = \dot{V}\rho C_p \Delta T \tag{6}$$

The term ΔT depends on the inside air temperature. This varies according to the total thermal loads and the thermal characteristics of trains. Consequently, the thermodynamic modeling of trains is needed. There are several works about the thermal modeling of trains [36]–[43], usually focused on passenger thermal comfort. According to thermodynamic theory, each train element can be modeled individually (furniture, doors, windows, walls, floor, etc.). However, it is a common practice to lump furniture mass to air mass, as well as to considerer all chassis structures as one. Apart from these considerations, the more individual thermal systems are considered, the more differential equations need to be solved, thus, more computational resources will be necessary. To avoid high computational cost, a second-order model is selected in this work. The model showed in Hofstädter *et al.* [43] is used, but adding more heat sources as follows.

Equation (7) describes the thermal modeling of the inner air of trains. This equation can be used to model each individual wagon air volume, but also for an average approach where all air volumes are aggregated. Here, TM_a represents the air thermal mass; T_a is the inside air temperature; T_o is the outside temperature, which it is considered constant along the train envelope; T_t is the temperature of the train body; U_{ao} and A_{ao} are the total thermal transmittance and the related area between inside and outside air, respectively; U_{at} and A_{at} are the total thermal transmittance and the related area between inside air and train body; $\dot{Q}_{HVAC}$ represents the heat power delivered by the HVAC system to provide thermal comfort; and $\dot{Q}_{mix\,1}$ is the sum of other thermal loads as passenger latent and sensible heats, radiation through windows, leakages, illumination inefficiency, etc. Depending on the desired precision of net thermal load, each one may be modeled individually. Consequently, materials, people behavior, and equipment characteristics may be considered. Note that equation (*7*) considers heat fluxes into the train air volume, however, it also works with outgoing heat fluxes. Moreover, the usage of negative $\dot{Q}_{HVAC}$ is because of the assumed direction of heat. Since the heat goes from outside to inside, the HVAC system operates in cooling mode.

$$TM_a \frac{dT_a}{dt} = \dot{Q}_{mix\,1} + U_{ao}A_{ao}(T_o - T_a) + U_{at}A_{at}(T_t - T_a) - \dot{Q}_{HVAC} \quad (7)$$

The behavior of outside temperature, T_o, depends on environmental conditions, contrary to T_t. The train body temperature, T_t, varies according to the body thermal mass TM_t, and related heat fluxes, as seen in equation (*8*). In this model, the mass of wheels, bogies, motors, etc. are lumped into a single mass. The $\dot{Q}_{mix\,2}$ describes radiation from surroundings, and heat exchanges with rails and ground. This term depends on local weather data and surrounding reflective characteristics. It can be defined by means of a highly detailed thermal modelling, or by adjusting its value to meet acceptable values of T_t.

$$TM_t \frac{dT_t}{dt} = \dot{Q}_{mix\,2} - U_{at}A_{at}(T_t - T_a) \quad (8)$$

The power $\dot{Q}_{HVAC}$ depends on how both thermal masses interact under specific thermal load and environmental conditions. If there are little heat gains and/or large thermal mass, the passenger thermal comfort will not be compromised and, therefore, the operation of $\dot{Q}_{HVAC}$ is not critical. The HVAC system can be operated by on/off logics [27], as well as by varying the compressor and/or blower performance [26]. The last approach would modify the amount of injected air ($\dot{V}$) as well as its thermodynamic characteristics.

Finally, trains and traction substations are modeled as controlled current sources, and voltage sources, respectively. The value of the current can be calculated by dividing the train electrical power (1) by the instantaneous catenary voltage, U_{cat}. The controlled current source is connected to the catenary as in Almaksour *et al.* [28]. However, although the impedance between traction substations and trains varies according to the movement of trains [44], this impedance variation can be neglected. This is only valid if the considered traction substations are supplied by the same grid feeders. Because, in grid frequency studies, the interaction between loads and the grid is described in terms of power, it is not strictly necessary to calculate the power managed by each traction substation, and the power seen by grid feeders is enough.

2.2. Electric Power System

Since the analysis of frequency behavior is the main focus, a primary frequency control scheme is selected to model power systems [1]. Here, an appropriate frequency-based description of power plants and loads is needed. Related to power plants, it is required to know their: per unit participation in the instantaneous dispatch of energy (ω_i), transient behavior [45], and speed regulator topologies. On the other hand, the modeling of loads implies their transient behavior, which must include their frequency response, commonly described by means of damping factors (D_{eq}). Equation (9) describes the relation between grid frequency deviations ($\Delta\omega_{eq}$) and load variations (ΔP_L). It can be seen how a load increment results in a frequency decrement. Moreover, the grid equivalent inertia (H_{eq}), imposed by its global rotational mass, and the load damping factor are inversely related to the grid frequency. The equivalent inertia of the *m* plants of the system can be calculated by equation (10), where H_i represents the i^{th} plant inertia constant. The presence of power plants in the energy dispatch, along with their inertias, stablishes the equivalent grid inertia. This equation helps to understand how the integration of renewable energy-based power plants can reduce the grid inertia. The terms $D_i(s)$ and $S_i(s)$ represent the frequency-based dynamic behavior and the operation scheme of speed controllers, respectively. The "s" stands for the Laplace operator.

$$\frac{\Delta\omega_{eq}(s)}{\Delta P_L(s)} = \frac{-1}{2H_{eq}s + D_{eq} + \sum_{i=1}^{m} \omega_i\, D_i(s)\, S_i(s)} \quad (9)$$

$$H_{eq} = \sum_{i=1}^{m} \omega_i H_i \quad (10)$$

Therefore, taking as an example the diagram presented by Ochoa *et al.* [46], adapted here as Figure 1, it is possible to use the previous equations to study the frequency deviations. The blocks labeled with "HG" contain the product of $D_i(s)$ and $S_i(s)$, as shown in equation (9). Any type on power plant can be represented in the diagram if its frequency-based dynamics is known [45]. Figure 1 also shows how the railway model can be integrated into the power system model. The railway model includes non-frequency dependent (NFD) and frequency dependent (FD) consumptions.

Additionally, in this work, railway consumption is considered as the only electrical load deviation (ΔP_L), although the presented model allows to include non-railway consumption. However, as primary frequency regulation is related to the first seconds after an event [9], just a part of the railway consumption profile is enough for the study. Apart from railway running consumption fluctuations, ΔP_L varies according to the HVAC system operation, which has been proposed to change depending on train air temperature and grid frequency deviations.

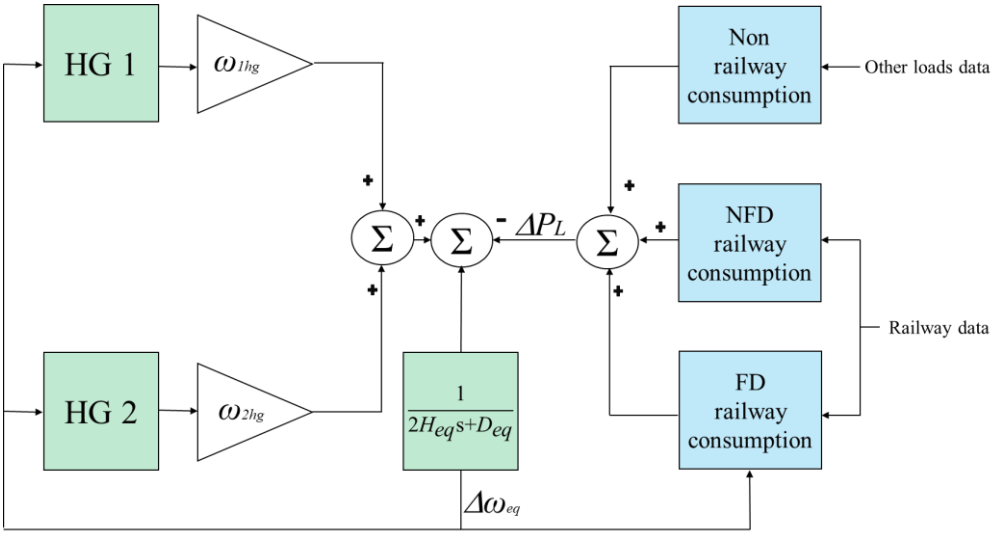

Figure 1. Example of the higher layer of a primary frequency control scheme integrating hydroelectric generators (HG), non-railway consumption, non-frequency dependent (NFD) railway consumption, and frequency dependent (FD) railway consumption.

The "FD railway consumption" block contains the subsystems needed to describe the HVAC system response to frequency deviations. As seen, the HVAC system normal response depends on railway thermal envelope and on its own topology. The "Railway data" input defines the required characteristics. Additionally, grid frequency deviations ($\Delta\omega_{eq}$) can modify the delivered heat power by modifying some of HVAC system operation parameters. Depending on HVAC system model detail, how frequency deviations affect the operation may vary. Equation (6) simplifies this relation. Thus, injected air flow and its temperature are the only parameters that can be modified (see Appendix A for more detail).

3. Case Study

According to the purpose of assessing the possibilities of using trains for contributing to frequency control, by considering their thermal inertias, a case study is presented. Several scenarios are set up, where the railway frequency control response is studied under different electrical events, and different train thermal characteristics. Although any railway technology can contribute to frequency control of a power system, a DC railway-based case study is considered.

3.1. Railway model based on Panama Metro Line 1

The railway system is inspired by the characteristics of the rolling stock and catenary system of Panama Metro Line 1 (PML1). PML1 is a double track system which operates at 1500 V_{DC}, has 14 passenger stations, and is fed from two connection points to the public grid. It distributes the AC power by means of an internal AC circuit to supply 8 traction substations. Some other useful data for modeling are: *A*, *B*, and *C* Davis coefficients are 2547.648 N, 21.6048 Nh/km, and 0.59 Nh^2/km^2, respectively; total train length, wagon width, and wagon height are 86.094 m, 2.71 m, and 3.859 m, respectively; the rated train mass ranges from 155875 kg to 245405 kg, depending on occupancy; the maximum and operating train speeds are 80 km/h, and 32.5 km/h, respectively; the dwelling time is from 20 s to 30 s; the headway in peak hours and off-peak hours is 120 s and 250 s, respectively; the catenary contact wire has a resistance of 0.177 Ohm/km at 20°C; the catenary has a copper equivalent section of 1400 mm^2; and the rail resistance is less than 0.04 Ohm/km.

For a completely accurate model, the information of the railway layout is needed. The profiles of slope, speed, and radius of curvature define the forces in equations (2)-(5). However, including these profiles can complicate even more the model elaboration, without adding relevant information to assess the railway frequency control contribution. Therefore, to reduce the computational cost, null slope and infinite curvature are considered. Moreover, any mechanical phenomenon, as the interactions pantograph-contact wire and wheels-rails, are neglected since their influence in the study is minimum. As a result, the speed profile is what mainly determines the train consumption. To solve equation (1), a standard circulation of PML1 is used, as showed in Figure 2. Here, the rated dwelling time and headway are considered. The resulting running is replicated to simulate the train transit along 5 passenger stations and 3 traction substations. As previously said, the time framework of primary frequency control is very short compared to train dynamics. Hence, to focus the resources on the frequency response study, an equivalent circulation of just 2 trains per track is considered. Figure 2 shows speed, acceleration, and displacement profiles of trains in both tracks. Here, the headway of 120 s and the dwelling time of 30 s can be seen. In addition, the 3 traction substations are fed by the same public grid feeder. Thus, the grid sees the totalized power consumption of the railway system.

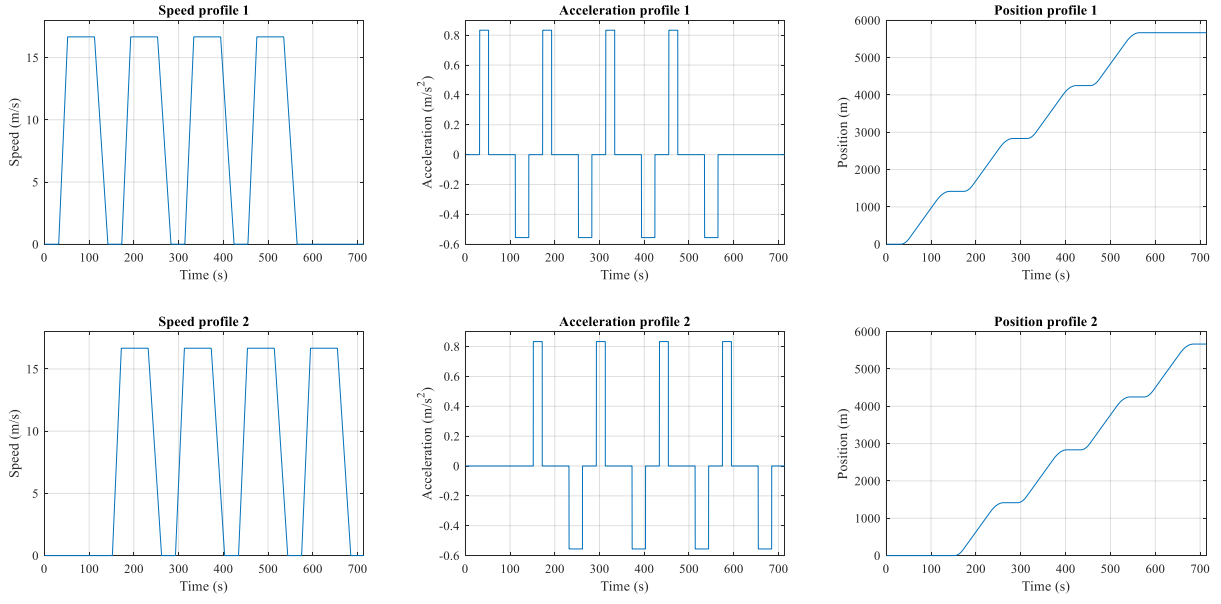

Figure 2. Considered profiles of speed, acceleration, and position of trains on both tracks. Upper row: profiles for the first train of each track. Lower row: profiles for second train of each track.

In relation to the train thermal characteristics, the work of Hofstädter *et al.* [43] is used to study several thermal configurations and how these influence on primary frequency control. So, the terms TM_a, TM_t, U_{at}, A_{at}, and U_{ao} of

equations (7) and (8) are easily obtained. Additionally, the PML1 train characteristics and the climate data are used to define A_{ao}, $\dot{Q}_{mix\,1}$, and $\dot{Q}_{mix\,2}$. This is, by considering the train geometry, a maximum Panamanian solar irradiance (1000 W/m^2), an occupancy relative to the maximum admissible train weight, etc., these terms are easily obtained. The variation of convective coefficients due to train speed is neglected. The thermal comfort zone ranges from 23.5°C to 28.5°C [47], based on a Panamanian neutral temperature of 26°C [48]. Each passenger represents a thermal load of 116.3 W. The HVAC system operates only in cooling mode due to the climate of Republic of Panama. The HVAC system is an inverter-based class, where the motor speed varies continuously. A mean coefficient of performance, COP_{mean}, of 3.4 are considered [38]. As exposed, the HVAC system is modeled as in equation (6), but disregarding technical restrictions that could depend on the capacities of blowers, compressors, and motors, among other devices. Hence, how the drives are continuously adjusted to meet comfort conditions is disregarded. Instead, a PI controller is used to minimize temperature deviations. Its output, along with injected air characteristics, define the HVAC heat power (6).

3.2. Electric Power System Model

The electric power system is modeled as in Ochoa [1]. This approach allows to obtain frequency-based results without developing complex models. As said, load variations seen by the grid are represented by the railway model, and, similarly, the electric system power plants are represented by two 180 MW hydroelectric groups. As in Ochoa [1] and Kundur [45], the dynamics of the power system is represented by a: droop of 5%, gate time constant of 0.2 s, transient droop of 4%, and water time constant of 1 s, being 180 MW the base power. There is a wide range of possible inertias depending on the size and technology of power plants. A representative inertia of 4.0 s is chosen for both hydroelectric power plants, and a typical load damping factor of 1% is used.

By applying the running profiles on Figure 2, railway characteristics in section 3.1, and equations (1)-(5), the power profile of Figure 3 is obtained, where a railway peak power consumption of about 18 MW can be seen. This means a 5% railway power penetration, compared to the installed capacity [49].

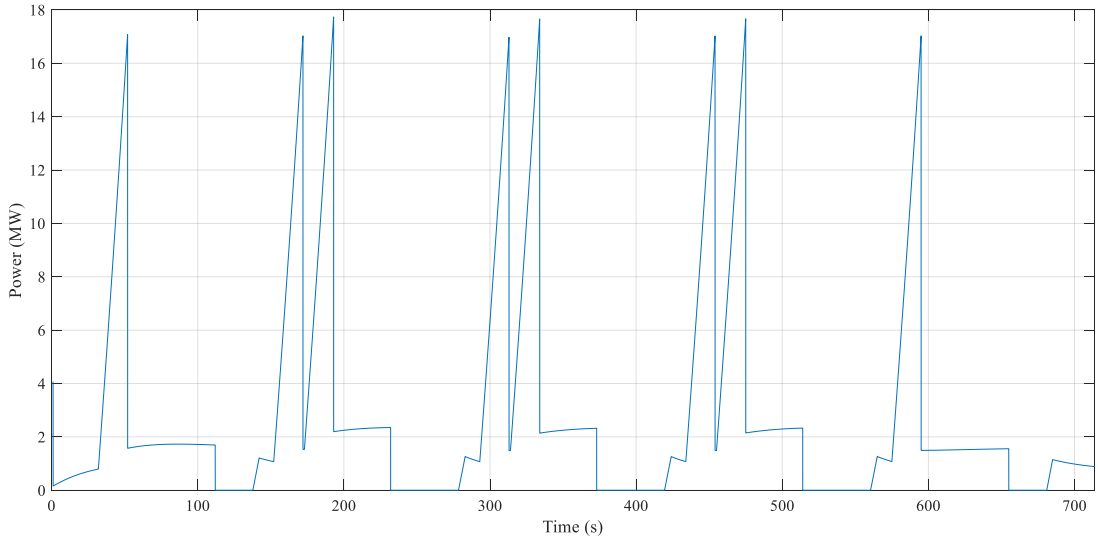

Figure 3. Railway consumption profile.

To study the interaction between the railway and the power system, six subcases are considered. Some of them study the response to sudden losses of loads and generation in the power system, and the other ones evaluate how railway can face frequency deviations due to its own consumption and the influence of thermal characteristics.

4. Results and Discussion

The railway and power system models are developed on Matlab/Simulink. A time step of 16.67 ms is used on discrete mode. All the results are based on a 60 Hz system, with an outside temperature between 35°C and 38°C, according to Panamanian climate on critical days [50]. The heat power developed by HVAC systems is oriented to maintain a neutral temperature (T_N) of 26°C in trains. Equation (11) shows the control method used to update HVAC setpoint temperature, T_{set}. Here, a frequency deviation, Δf, stablishes a temperature variation rate by means of a droop control, D_{th}, and a dimensionless droop factor, k_D.

$$T_{set} = T_N - \Delta f \, D_{th} \, k_D \tag{11}$$

Consequently, under positive frequency deviations, which can be caused by sudden load shedding and/or generation increase, the HVAC system reduces its setpoint temperature, therefore, providing an increment of power consumption. Otherwise under negative frequency deviations, which can be caused by sudden increment of load or sudden generation loss, the HVAC system reduces its power consumption. To obtain and adequate value for the droop, it has to be taken into account that the frequency interaction between railway and power system must meet some standard criteria. According to the standard in [51], a maximum frequency deviation of 800 mHz, and a maximum *quasi*-steady state deviation of 180 mHz are allowed. Due to the admissible temperature (±2.5°C) and frequency (±800 mHz) bands, a value of D_{th} = 3.125 °C/Hz has been chosen. The droop factor, k_D, facilitates to change the aggressivity of the droop control for analysis purposes. In addition, a dead band of ±17 mHz is included [52].

In the following subcases, the figures display: grid frequency, rate of change of frequency (ROCOF), air train temperature, heat power delivered by HVAC system, and load seen by the grid. The thermal behavior of each train is considered identical to speed up modeling time, except in subsection 4.6 where different thermal states of trains are considered. The 11th thermal envelope configuration showed in Hofstädter *et al.* [43] is used, except in sections 4.4 and 4.5 where multiple configurations are assessed.

4.1. Response to power system disturbances: sudden load shedding

Figure 4 shows the responses following a load shedding of 0.1 p.u. in the power system, with different droop factors. These factors allow to assess the system response from 0% (i.e., with no contribution of trains to frequency control) to 500% of the droop standard value, D_{th}. As expected, larger droops provide faster frequency control, and reduce maximum deviations. The droop at 500% achieved a maximum frequency deviation reduction of 16.5 mHz, compared to the 0% case, and the ROCOF variations among cases are negligible. These results are obtained by means of increasing almost three times the heat power. The temperature deviation ranges from 0.05°C to 0.23°C, not affecting the passenger comfort.

As seen in Figure 4, the behavior of all cases is similar. When the event occurs, the droop control reduces the temperature setpoint to provide frequency control. As soon as the event is managed by the power plant speed controller, the train controllers stop their participation, and each HVAC system return to their base operation. However, those cases with an aggressive droop control remain with a noticeable temperature deviation that will be slowly corrected by the HVAC system normal operation (not shown in Figure 4). The thermal inertia role is clearly observed in the temperature behavior since temperature deviations are minimum under considerable heat power variations.

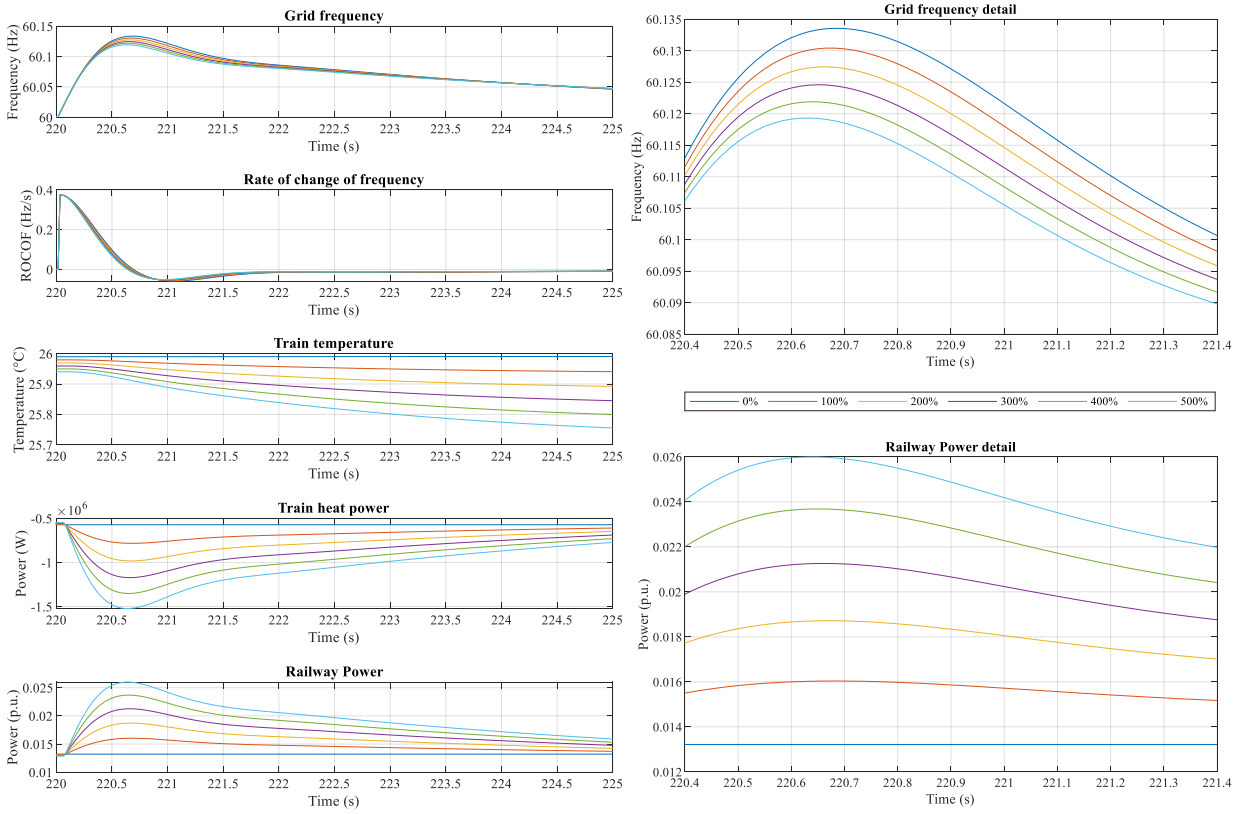

Figure 4. Railway and power system responses following a sudden load shedding event.

4.2. Response to power system disturbances: sudden generation unit loss.

A power plant with an inertia constant of 2.0 s and power capacity of 0.1 p.u. is suddenly disconnected at t = 220 s. This event reduces the grid frequency and the capacity of frequency stabilization since the equivalent system inertia is also reduced. Figure 5 shows this case, where the benefits of using more aggressive droops can also be noticed. The ROCOF variations among cases are also negligible. The maximum frequency deviation reduction is 9.6 mHz compared to the case with 0% droop. However, the reductions of droop at 400% and 300% are also 9.6 mHz, because in these three cases the consumption reduction has reached the lower level, i.e., a consumption of 0 W. Therefore, the benefits of using higher droop factors are restricted by the HVAC system operation range. This can be seen in "Train heat power" and "Railway power" plots. Here, some curves reached a constant power zone defined by other auxiliary consumptions. Thus, the delivered heat rate is affected, and temperatures remain close to each other. As a result, a temperature deviation between -0.05°C and 0.12°C is found during the event, which is lower than the previous case.

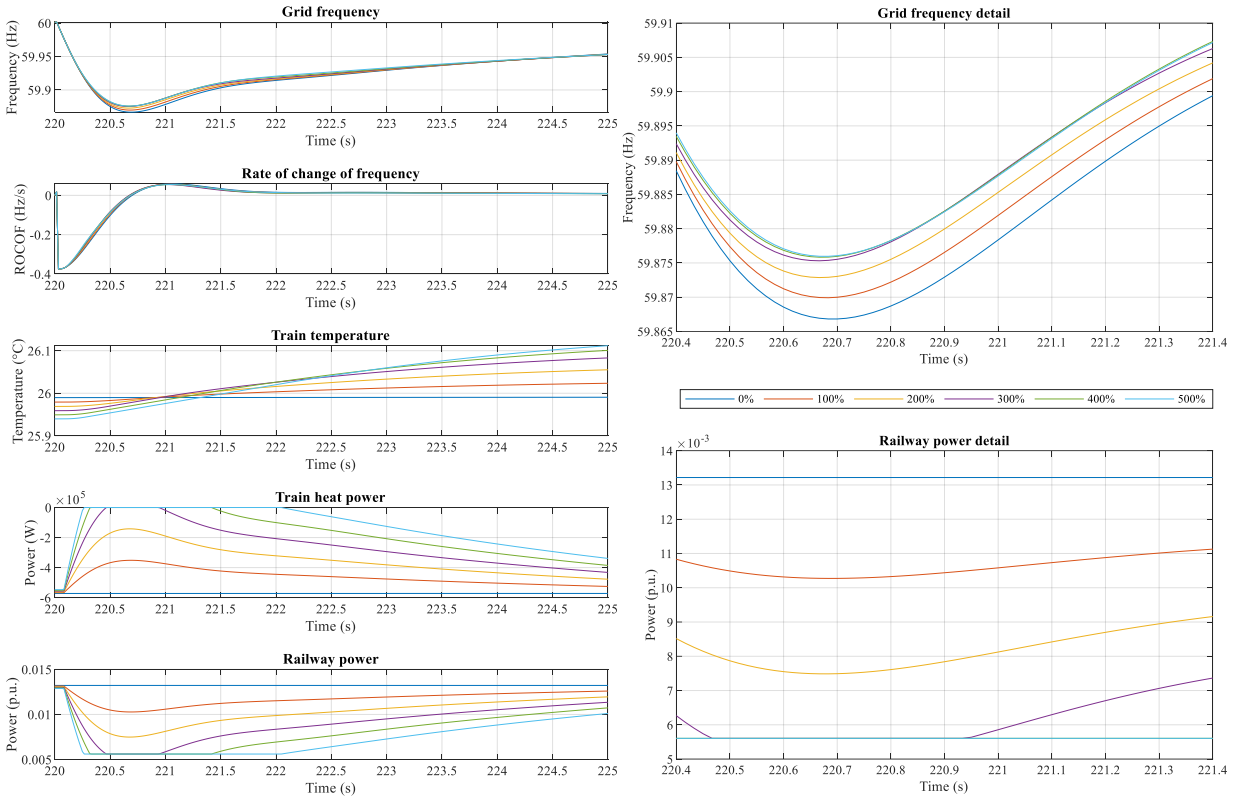

Figure 5. Railway and power system responses following a sudden generation loss event.

4.3. Response to railway disturbances

The power system can be subjected to disturbances that impact on frequency, as described in subsections 4.1 and 4.2. But the normal variations of consumption of trains, as described in Figure 3, also affect the power system frequency. The proposed control technique also contributes to mitigate these frequency variations. For example, the left part of Figure 6 shows the behavior of the variables of interest in the period from t = 311 s to t = 317 s. As shown in Figure 3, the railway consumption has a sudden drop at t = 311 s, from 17 MW to 1.5 MW, followed by a ramp increase from t = 312 s on. The right part of Figure 6 shows a zoomed part of the system frequency and railway power curves, where a maximum frequency deviation reduction of 11.8 mHz can be seen, compared to the case with 0% droop. Since disturbances are smaller than the ones in subsection 4.1, reductions are also smaller. Nonetheless, still higher droops provide better frequency control.

In relation to the thermal behavior, it is remarkable that the temperature deviation ranges from -0.02°C to 0.08°C among droop cases. This is coherent with the delivered heat power, which is lower than in subsection 4.1. In the previous 311 s, many load and frequency variations occurred, what led to a different thermal evolution in each case. This explains why at the beginning of the period shown in Figure 6 the temperatures are different, but due to the same frequency disturbance all the temperatures evolve similarly.

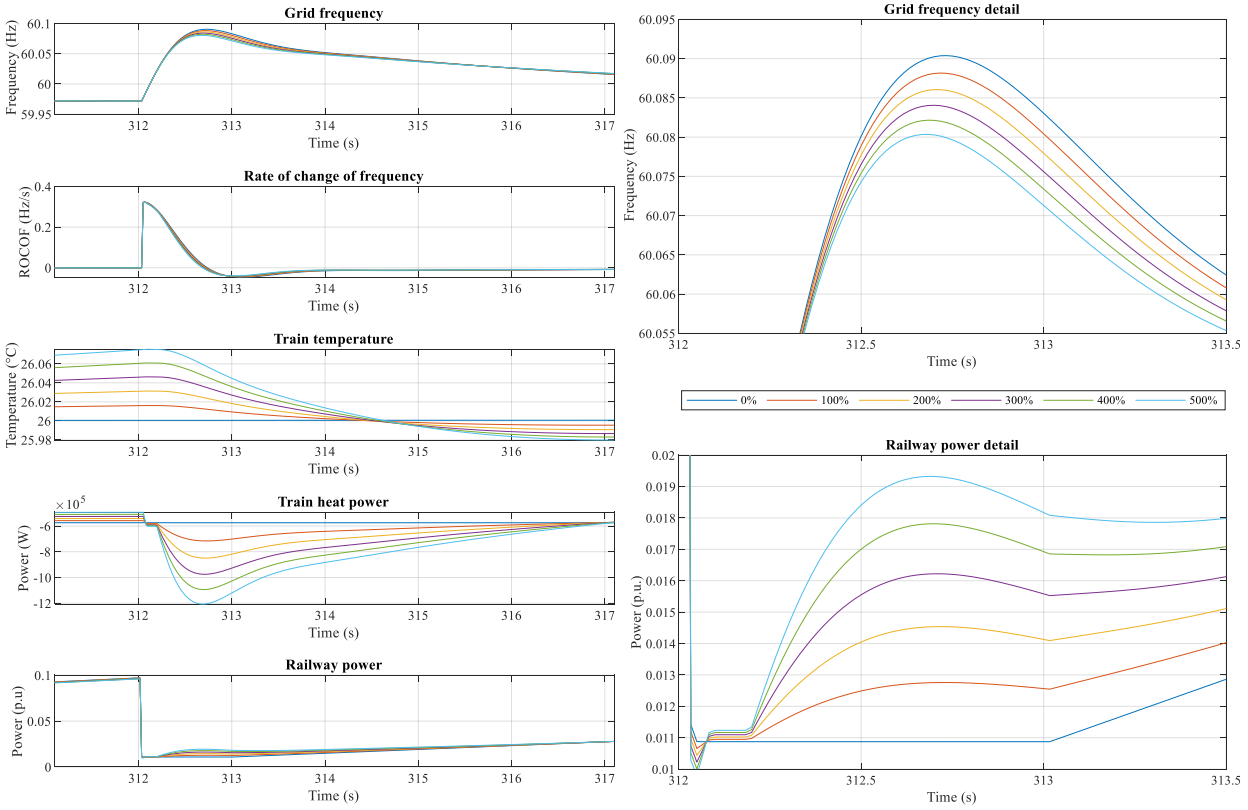

Figure 6. Railway and power system responses to normal railway consumption variations.

4.4. Response to railway disturbances: different thermal envelopes

This subsection shows how the proposed frequency control strategy impacts the thermal comfort of passengers depending on the thermal characteristics of trains. To do so, the aggressivity of the frequency controller is kept at 300%, and the thermal behavior is assessed with thirteen different trains, as defined in Hofstädter *et al.* [43]. The terms in equations (7) and (8) are described in [43] as follows: $TM_t = C_{veh}$, $TM_a = C$, $U_{ao} = k$, and $U_{at}\,A_{at} = k_{veh}$. Table 1 compiles all these values. The usage of these equations attempts to speed up the study of the influence of thermal inertia in grid frequency control without the need of exhaustively describing the envelope of trains.

Table 1. Thermal envelopes of trains by Hofstädter *et al.* [43].

Envelope name	U_{ao} (W/m^2K)	TM_a (J/K)	$U_{at}\,A_{at}$ (W/K)	TM_t (J/K)
Tram 1	2.5	3.0×10^7	246	1.7×10^7
Tram 2	3.2	1.8×10^7	974	1.0×10^7
Metro 1	2.8	9.4×10^6	464	1.9×10^7
Metro 2	3.1	9.2×10^6	199	9.6×10^6
Metro 3	2.9	8.0×10^6	47 831	5.7×10^6
Metro 4	2.4	4.6×10^6	230	1.3×10^7
Metro 5	2.9	1.1×10^7	5 479	2.3×10^7
Regio 1	1.7	4.3×10^7	484	4.6×10^6
Regio 2	1.3	6.4×10^6	1 366	3.1×10^7
Regio 3	2.0	3.6×10^6	217	1.1×10^7
Regio 4	1.7	1.3×10^7	907	3.7×10^7
Main 1	1.4	7.2×10^5	93 627	3.9×10^6
Main 2	1.6	2.6×10^6	564	2.4×10^7

Figure 7 shows the detail of the variables of interest in the same period than subsection 4.3. It is remarkable how the variation of train thermal characteristics practically does not influence the power system frequency behavior under the same control scheme and load conditions. On the contrary, the thermal behaviors of trains are different among cases. By considering the configuration with the worst frequency control, Main 1 (Ma1), a temperature difference between -0.02°C and 0.31°C is found in the period shown in Figure 7, compared to the one with the best frequency control, Regio 2 (R2). The train heat power curves also show the difference on performance. These differences can be explained by inspecting the parameters in Table 1. The term U_{ao} influences the heat gains between inside and outside air temperatures. The term $U_{at}\,A_{at}$ determines the heat gains between inside air and train body temperatures. The terms TM_t and TM_a represent the thermal mass of trains and inside air, respectively. As seen in Table 1, all U_{ao} terms have the same order of magnitude, in contrast to the other terms. $U_{at}\,A_{at}$, TM_t, and TM_a present noticeable differences among configurations. However, the temperature difference between inside air and train body is naturally small, therefore, the influence of $U_{at}\,A_{at}$ is expected not to be much relevant. The inertia of train body ranges within one order of magnitude among configurations, thus not being much relevant either. From these considerations, it is understandable why Main 1 (Ma1) presents the worst thermal behavior. This configuration has the lowest air and train body thermal inertias, and the highest value of $U_{at}\,A_{at}$, i.e., the highest heat gains, but the lowest capacity to manage them. This also explains why Main 1 (Ma1) delivers the lowest heat power. Because of the low thermal inertia, the HVAC system does not require too much energy to modify the inside air temperature.

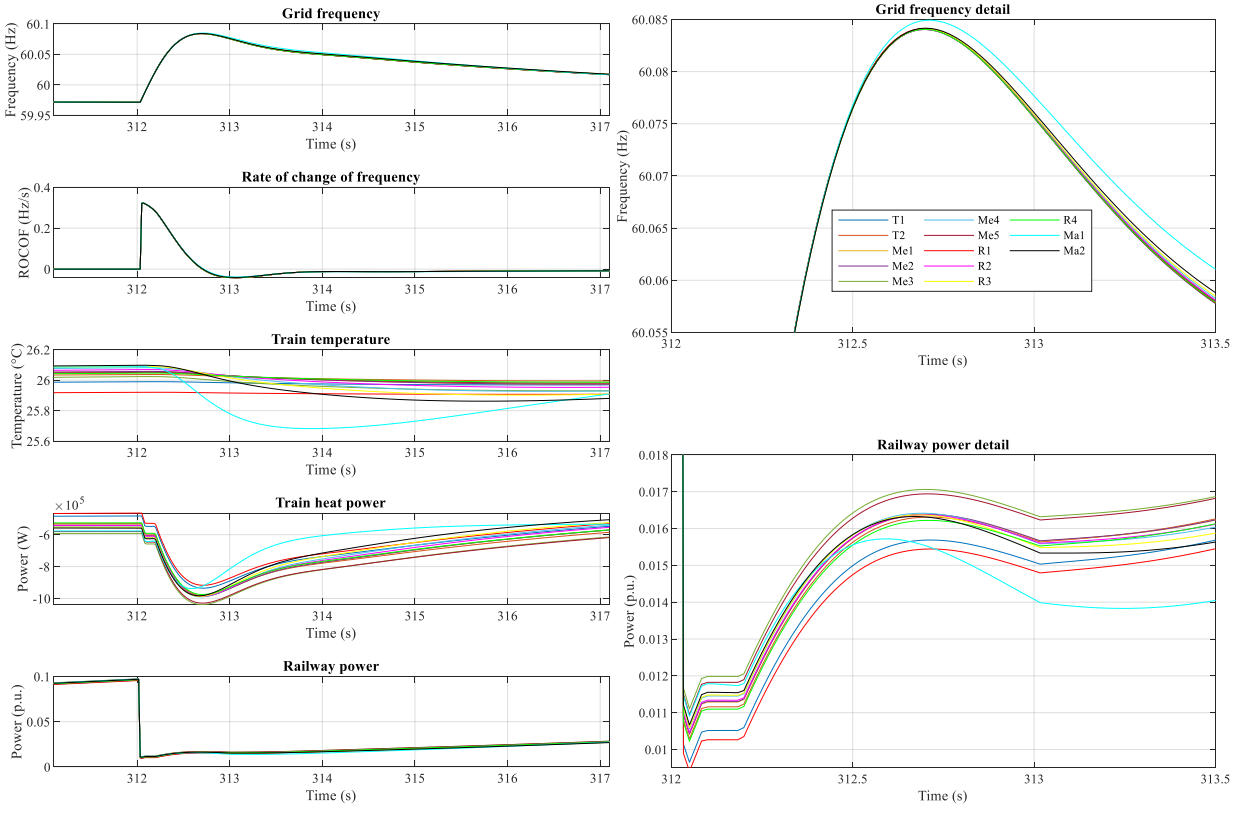

Figure 7. Railway and power system responses to normal railway consumption variations. Sensitivity to different thermal envelopes of trains.

Finally, it is concluded that high thermal inertias provide even more frequency control possibilities. The higher the thermal inertia, the lower the temperature fluctuation, and, therefore, the wider the HVAC system operation energy band. As mentioned before, this approach is based on the difference between thermal and frequency dynamics. Having a slower thermal dynamics allows a more intensive contribution of railway to frequency control within the margins of passengers comfort.

4.5. Response to railway disturbances: two thermal envelopes with different droop control

In subsection 4.4, different thermal envelopes were compared under the same frequency control scheme. According to results, Regio 2 (R2) achieved an average and maximum extra frequency control of 1.1 mHz, and 3.0 mHz, respectively, compared to Main 1 (Ma1). Both configurations under the same droop of 300%. This section compares both configurations with different droops from 300% to 600%. It is expected to see how much frequency control can be achieved by increasing control aggressivity.

Figure 8 shows the results of varying thermal characteristics and droop control configurations. Regio 2 (R2) has little temperature variations among droop cases and along time. Due to its high thermal inertia, the different droop controls did not lead to considerable temperature variations and, therefore, higher heat power is delivered and maintained. Note how in 5 s the Regio 2 (R2) temperatures only decreased a maximum of 0.22°C, contrary to Main 1 (Ma1) where temperatures fell more than 0.78°C, thus, demanding less heat power and electric consumption. Here, thermal inertias mainly determine the range of thermal behavior. Within each thermal configuration, similar tendencies about increasing droop control are visualized. The higher the droop aggressivity, the higher the temperature and heat power variations.

In heat power and railway power behaviors, due to thermal inertias, Regio 2 (R2) remains with higher powers, where droop cases differ little among them. In Main 1 (Ma1) lower powers remain after the event and thermal behavior of cases tend to be similar. However, during the transient period, between the first two seconds after the action of droop control, the highest thermal inertia and droop coefficients seem to not individually define the power behavior, which also constraints the frequency response. Figure 8 shows a detail of the frequency behavior. As seen in previous sections, the highest thermal inertia with the most aggressive droop control (R2-600%) provides the greatest frequency reduction. Also, the lowest thermal inertia with the least aggressive droop control (Ma1-300%) provides the lowest frequency deviation reduction. However, there are some pairs of curves which did not fit the expected: “R2-500%” vs. “Ma1-600%”, “R2-400%” vs. “Ma1-500%”, and “R2-300%” vs. “Ma1-400%”. During the transient period, the “R2”-based cases with more aggressive droop control behaved clearly better than “Ma1”-based cases with less aggressive control, with the exception mentioned pairs, where “Ma1”-based cases with higher droop control were temporary better. After the transient, toward the steady-state response, the effect of thermal inertia on curves predominates. This observed behavior suggests that increasing control aggressivity can compensate transiently the lack of the thermal inertia.

The results show that an envelope with 8.9 times thermal inertia, under the same control scheme, can provide an extra maximum reduction of 5.2 mHz on frequency deviations. In addition, if extreme cases are compared, “R2-600%” vs. “Ma1-300%”, an average and a maximum frequency deviation reduction of 2.4 mHz and 8.2 mHz are obtained, respectively. This represents an improvement to behaviors in subsection 4.4.

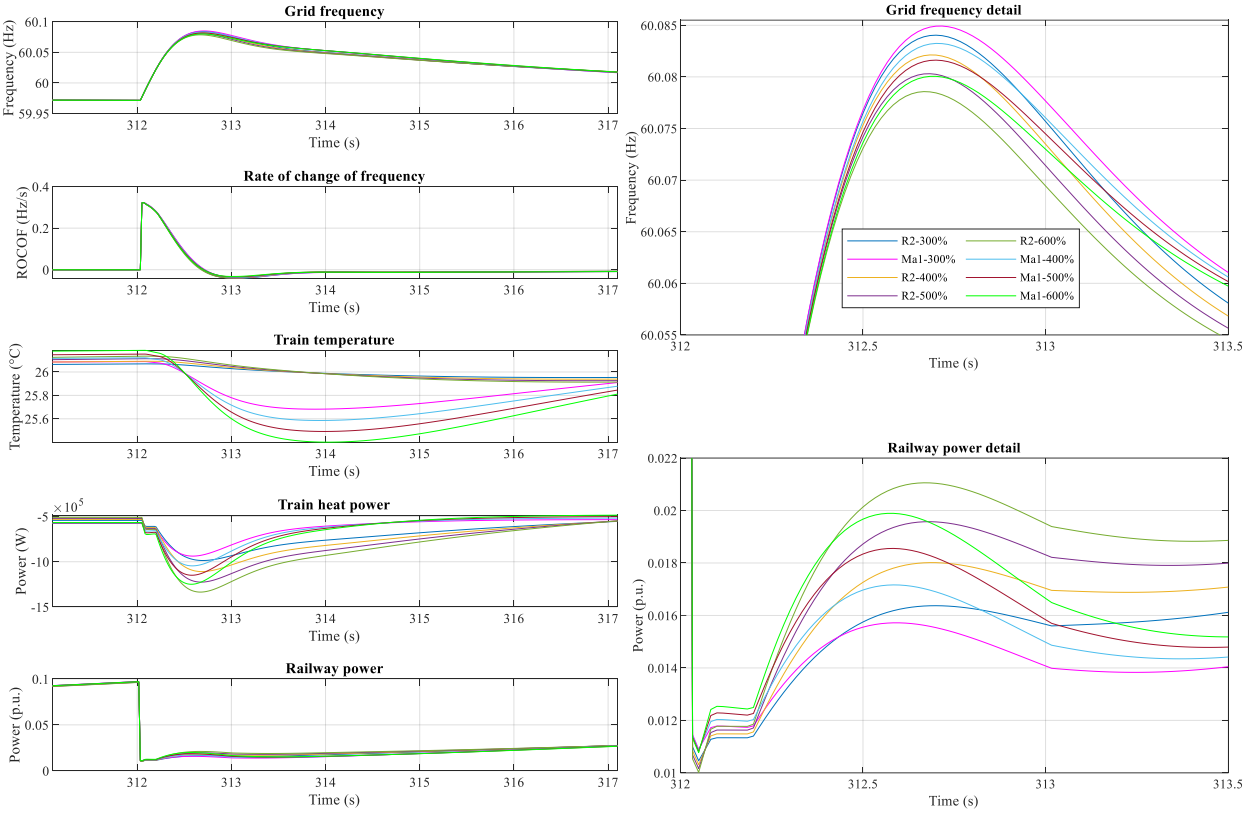

Figure 8. Railway and power system responses to normal railway consumption variations. Combined sensitivity to thermal configurations and droops.

4.6. Response to power system disturbances: sudden load shedding and individual train thermal modelling

All the previous subsections considered that all trains shared the same thermal status. This approximation is reasonable for a model simplification to focus the study on the grid frequency control. However, it is interesting to see how results vary when a higher complexity in the thermal modeling of trains is used. This is, instead of assuming a representative train thermal behavior to trigger the frequency control in all trains, the individual thermal behavior of each train determines its contribution.

To distinguish each train thermal behavior, a variation of solar radiation while trains are on passenger stations is studied. Also, the trains of each track transport different number of passengers. Still, all trains have the same thermal configuration. By means of headway, dwelling time, and new considerations, a different net heat gain at each train is obtained. Figure 9 shows the results of the individual thermal modeling without the action of droop control. As seen, during the entire circulation, the temperature remains practically constant with a maximum deviation of 0.55°C. Among individual temperatures of trains, a deviation band of 0.8°C ~ 0.6°C is found. Since each train temperature behavior is almost identical, the resulting average temperature curve has little differences. The heat power developed by each train exposed how thermal requirement of trains vary according to their location (variation of radiation) and their track (variation of number of passengers). However, since the individual and average temperature responses are very similar, it is admissible to consider the heat power variations almost irrelevant.

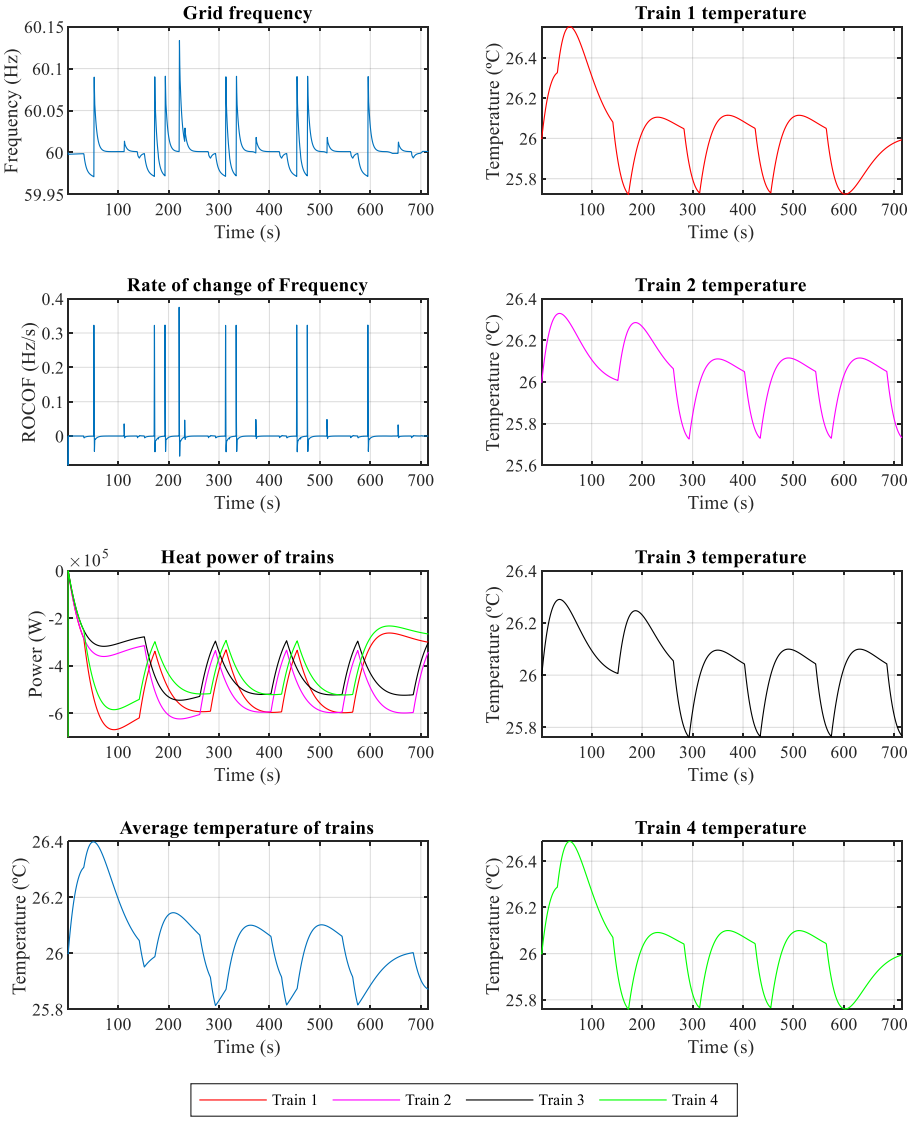

Figure 9. Railway and power system responses following a sudden load shedding event. Individual train thermal behavior. Null droop control.

The same analysis made in subsection 4.1 is carried out, and the results are showed in Figure 10. Here, each HVAC system provides different power variations to support frequency control, but the heat power plot is an average curve. The similarities between Figure 10 and Figure 4 are remarkable, where both present a maximum reduction of 16.5 mHz in grid frequency, comparing their responses of 500% droop with 0% droop. Related to frequency-based events, an individual train thermal modeling does not provide much more information.

About thermal behavior, a maximum temperature difference between droop cases of 0.2334 °C (Figure 10) is found. In subsection 4.1 the difference was 0.2352°C, which represents a neglectable difference of 0.0018°C between the “representative train-based control” and the “individual train-based control”. This suggests that stablishing a single train as the thermal reference for triggering the control is a valid approximation for this kind of studies. Moreover, for real-time applications on realistic trains, it can also be valid to measure the thermal state of one train and using it for triggering all the train frequency controls. However, for thermal comfort assessment in trains, it is not recommended to simplify thermal modeling.

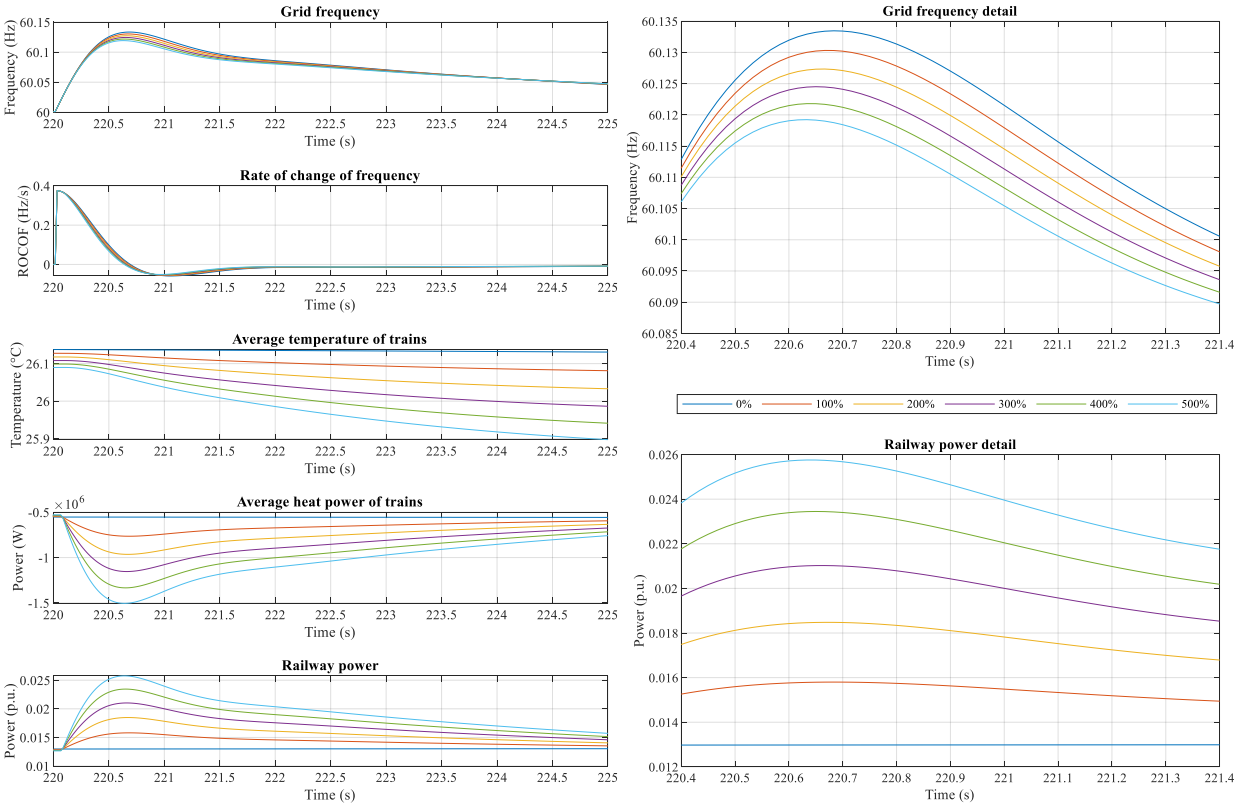

Figure 10. Railway and power system responses following a sudden load shedding event. Average train thermal behavior.

5. Conclusions

The contribution of non-conventional systems to grid ancillary services has increased its relevance due to the displacement of large conventional power plants from the energetic matrix. Therefore, new methods and approaches, applied to generators and consumers, have been developed.

Railway systems have been barely considered to provide these services. Only one work has been found, and it was based on modifying the circulation of trains by means of considerable complex procedures. Thus, in this paper, we propose a novel framework for implementing a railway contribution to frequency control. It consists of varying HVAC system operation according to frequency deviation and the thermal comfort of passengers.

To study the thermal comfort of passengers, a thermodynamical modeling of trains is needed. Hence, apart from conventional electric-dynamic modeling of trains and electrification system, a thermal modeling of rolling stock is required. More precisely, a load-frequency control model of the electric power system is coupled to the resulting railway system model to represent the interaction between thermal and frequency dynamics.

The results show the capacity of contribution to primary frequency control under external events, as sudden load shedding and generation loss, and power variations due to normal railway consumption. A droop control based on the relation of grid frequency and thermal comfort band is used to exemplify the action of HVAC systems to support grid frequency without risking thermal comfort. In all cases, the simulation results showed a very little variation on temperature while supporting frequency. Also, the study presented about the effect of thermal inertia and droop control aggressivity allows to confirm that higher thermal inertias can provide more frequency control, and the robustness of

droop control can increase even more these possibilities. Therefore, it is appropriate to conclude that this approach can have a great potential on contributing to primary frequency control to grid.

The results from subsection 4.6 allow to conclude that triggering the frequency control method by considering the thermal behavior of a single train, instead of computing each train thermal status, provides very similar results on frequency dynamics. However, the temperature differences between models can be relevant for thermal comfort studies. Thus, for frequency control studies, it is admissible to simplify the multi-train thermal modeling, but for thermal comfort studies might be not recommended.

It is remarkable that the relative amplitudes of events, railway consumption, and system inertia define the contribution of railway to frequency control. For larger railway systems, a more relevant contribution can be achieved. Furthermore, in future power systems, the tendency is that more and more loads and generators will be incorporated to grid frequency control tasks. The contribution of each piece of equipment (generator or load) separately is not significative, but the aggregation of all of them will have an effective impact on frequency control. Thus, the presented approach is expected to contribute toward this aim.

This paper has demonstrated the technical feasibility of using the thermal inertia of trains for contributing to the power system frequency control without affecting scheduling. Notice that several model simplifications have been done. Power system model can consider more realistic dynamics on energy supply/consumption. Railway system model, electrical and thermal, can include other aspects such as power converters topologies, HVAC thermal circuit restrictions, occupants' behavior, multidimensional wagon thermal model, among others. Then, this can be the basis for further analysis, including more detailed technical aspects and economic considerations.

Credit authorship contribution

Jesús Araúz: Conceptualization, Methodology, Software, Validation, Formal analysis, Investigation, Resources, Data Curation, Writing-Original Draft, Writing-Review & Editing, Visualization, Funding acquisition. **Sergio Martinez**: Conceptualization, Methodology, Formal analysis, Resources, Writing-Review & Editing, Supervision, Project administration, Funding acquisition.

Declaration of competing interest

The authors declare no conflict of interest.

Acknowledgments

The authors would like to thank the company "Metro de Panamá" and the "Universidad Tecnológica de Panamá" for providing the information of Panama Metro Line 1. Also, they thank to the Department of Automation, Electrical and Electronics Engineering, and Industrial Informatics of Universidad Politécnica de Madrid for allowing the use of computers.

This research has been funded in part by the Spanish national research agency Agencia Estatal de Investigación, grant number PID2019-108966RB-I00 /AEI/ 10.13039/501100011033.

Appendix A.

Figure A.1 represents the connection between the model in Figure 1 and the extended diagram of the "FD railway consumption" block. It can be seen how the HVAC system modifies its output according to frequency deviations. Moreover, as well as the railway data input, the train inner air temperature (Ta) is still defining the developed heat power. The composition of the "FD railway consumption" subsystem requires the interaction of two train subsystems:

thermal envelope and HVAC system. At the same time, these ones also require the interaction of two more subsystems. It is worth mentioning that the amount of system interactions depends on the detail of models.

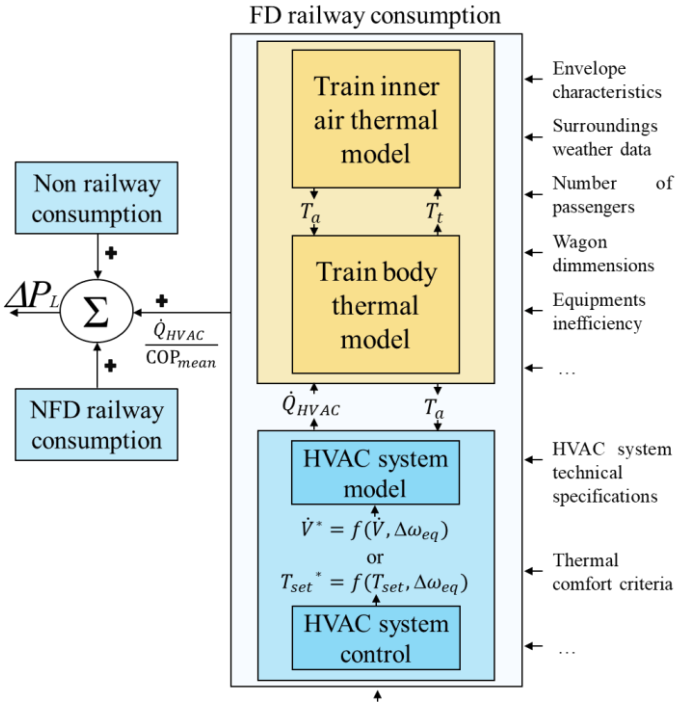

Figure A.1. FD railway consumption model detail. * denotes those parameters modified by the frequency control.

Apart from detailing HVAC system model and control, a stability analysis can be of interest. In this work, time-based equations have been used to describe every railway subsystem. To speed up the stability analysis, the Simulink application Control system designer has been used. This allows to plot some frequency-based graphic representation and the system response under common inputs (impulse, step). The application interface allows to choose signals and their location on the system. The heat power delivered by the HVAC system was selected as the output, while the frequency deviation was selected as the input.

Figure A.2 and Figure A.3 validate the stability of the exemplified HVAC system control. By means of Bode diagram, Figure A.2 shows the stability of the closed loop response. The results were obtained for $k_D = 5$. At $k_D = 1$, the gain margins are 14 dB less negative. The pole-zero map of Figure A.3 shows that all points are on the negative side of the real axis, meaning the system has a stable behavior. The imaginary part of poles represents the little oscillations on delivered heat power. The responses under common inputs are not presented here, as in the case study, several possible scenarios were considered, some of them being step perturbations. The stability under real possible cases was already reported in the results section. It should be mentioned that the stability margin relies on which control is implemented and how it is calibrated. The viability of implementing the proposed approach may depend on controls and on all the mentioned technical details.

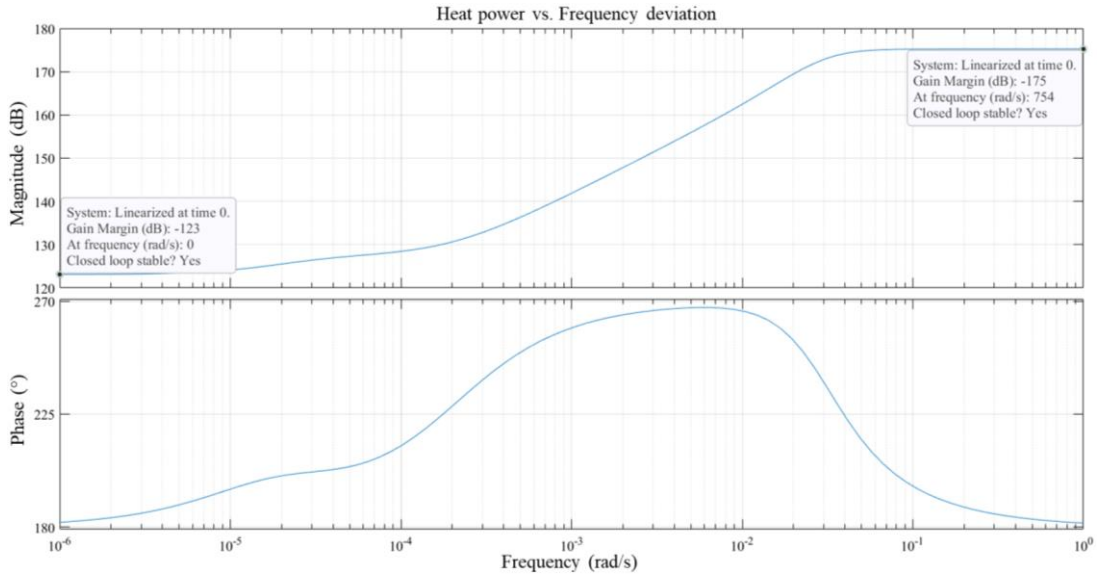

Figure A.2. Bode diagram (magnitude and phase). Stability analysis of the HVAC system frequency-based control.

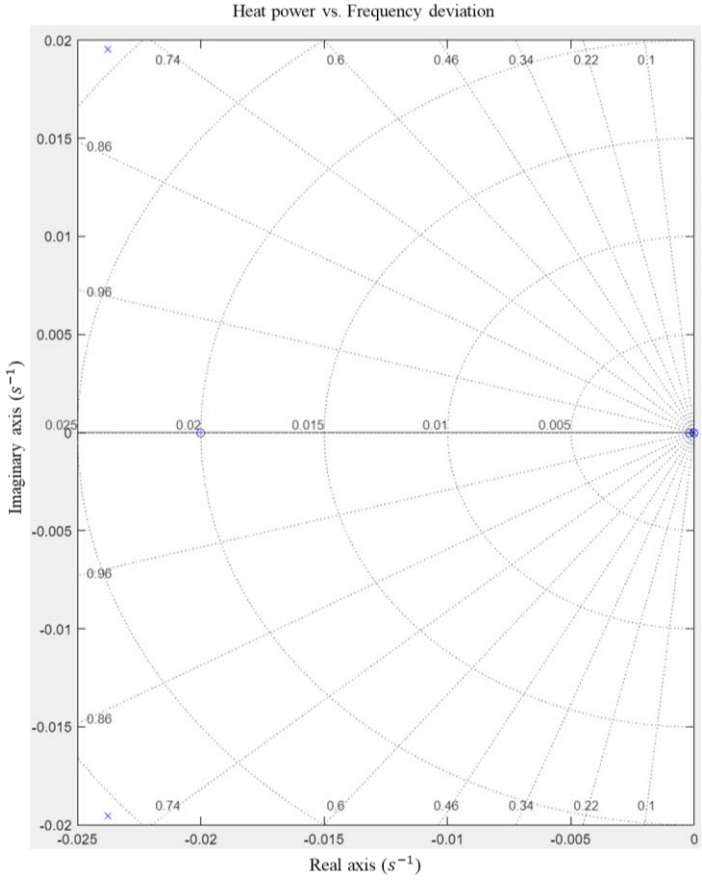

Figure A.3. Pole-zero map. Stability analysis of the HVAC system frequency-based control. "o" represents zeros and "x" poles.

References

[1] D. Ochoa and S. Martinez, “Contribución de los aerogeneradores de velocidad variable al control primario de frecuencia en sistemas de energía eléctrica,” Universidad Politécnica de Madrid, 2019.

[2] R. Teodorescu, M. Liserre, and P. Rodríguez, *Grid Converters for Photovoltaic and Wind Power Systems*, 1st ed. United Kingdom: John Wiley & Sons, Inc, 2011.

[3] D. Ochoa and S. Martinez, “Fast-Frequency Response Provided by DFIG-Wind Turbines and its Impact on the Grid,” *IEEE Transactions on Power Systems*, vol. 32, no. 5, pp. 4002–4011, 2017, doi:10.1109/TPWRS.2016.2636374.

[4] D. Ochoa and S. Martinez, “Frequency dependent strategy for mitigating wind power fluctuations of a doubly-fed induction generator wind turbine based on virtual inertia control and blade pitch angle regulation,” *Renew Energy*, vol. 128, pp. 108–124, 2018, doi: 10.1016/j.renene.2018.05.047.

[5] A. Golieva, “Low Short Circuit Ratio Connection of Wind Power Plants,” Norwegian University of Science and Technology, 2015.

[6] S. Julien, A. Sajadi, and B. M. S. Hodge, “Hierarchical Control of Utility-Scale Solar PV Plants for Mitigation of Generation Variability and Ancillary Service Provision,” *IEEE Trans Sustain Energy*, vol. 3029, no. c, pp. 1–13, 2022, doi:10.1109/TSTE.2022.3149451.

[7] M. Pierro, R. Perez, M. Perez, D. Moser, and C. Cornaro, “Imbalance mitigation strategy via flexible PV ancillary services: The Italian case study,” *Renew Energy*, vol. 179, pp. 1694–1705, 2021, doi: 10.1016/j.renene.2021.07.074.

[8] G. C. Kryonidis *et al.*, “Ancillary services in active distribution networks: A review of technological trends from operational and online analysis perspective,” *Renewable and Sustainable Energy Reviews*, vol. 147, no. May, p. 111198, 2021, doi: 10.1016/j.rser.2021.111198.

[9] U. Tamrakar, D. Shrestha, M. Maharjan, B. P. Bhattarai, T. M. Hansen, and R. Tonkoski, “Virtual inertia: Current trends and future directions,” *Applied Sciences (Switzerland)*, vol. 7, no. 7, pp. 1–29, 2017, doi:10.3390/app7070654.

[10] L. Meegahapola, P. Mancarella, D. Flynn, and R. Moreno, “Power system stability in the transition to a low carbon grid: A techno-economic perspective on challenges and opportunities,” *Wiley Interdiscip Rev Energy Environ*, vol. 10, no. 5, pp. 1–27, 2021, doi:10.1002/wene.399.

[11] P. Carroll *et al.*, “Development of network codes to facilitate the energy transition,” in *9th International Conference on Smart Grid, icSmartGrid 2021. June 29-July 1*, 2021, pp. 63–67, doi:10.1109/icSmartGrid52357.2021.9551230.

[12] C. Gokhale-welch and S. Stout, “Key considerations for adoption of technical codes and standards for battery energy storage systems in Thailand,” USA, 2021.

[13] M. Hussain and Y. Gao, “A review of demand response in an efficient smart grid environment,” *Electricity Journal*, vol. 31, no. 5, pp. 55–63, 2018, doi: 10.1016/j.tej.2018.06.003.

[14] A. R. Jordehi, “Optimisation of demand response in electric power systems, a review,” *Renewable and Sustainable Energy Reviews*, vol. 103, no. July 2018, pp. 308–319, 2019, doi: 10.1016/j.rser.2018.12.054.

[15] W. Huang, N. Zhang, C. Kang, M. Li, and M. Huo, “From demand response to integrated demand response: review and prospect of research and application,” *Protection and Control of Modern Power Systems*, vol. 4, no. 1, p. 13, 2019, doi:10.1186/s41601-019-0126-4.

[16] S. Yumiki *et al.*, “Autonomous vehicle-to-grid design for provision of frequency control ancillary service and distribution voltage regulation,” *Sustainable Energy, Grids and Networks*, vol. 30, Jun. 2022, doi: 10.1016/j.segan.2022.100664.

[17] M. Ledro, L. Calearo, J. M. Zepter, T. Gabderakhmanova, and M. Marinelli, “Influence of realistic EV fleet response with power and energy controllers in an EV-wind virtual power plant,” *Sustainable Energy, Grids and Networks*, vol. 31, Sep. 2022, doi: 10.1016/j.segan.2022.100704.

[18] A. Blatiak, F. Bellizio, L. Badesa, and G. Strbac, “Value of optimal trip and charging scheduling of commercial electric vehicle fleets with Vehicle-to-Grid in future low inertia systems,” *Sustainable Energy, Grids and Networks*, vol. 31, Sep. 2022, doi: 10.1016/j.segan.2022.100738.

[19] C. Diaz-Londono, C. A. Correa-Florez, J. Vuelvas, A. Mazza, F. Ruiz, and G. Chicco, “Coordination of specialised energy aggregators for balancing service provision,” *Sustainable Energy, Grids and Networks*, p. 100817, Dec. 2022, doi: 10.1016/j.segan.2022.100817.

[20] International Energy Agency (IEA) and International Union of Railways, “Railway Handbook 2017,” IEA member countries, 2017. ISBN: 9782746126626. [Online]. Available: www.uic.org.

[21] H. Yang *et al.*, “Coordinated demand response of rail transit load and energy storage system considering driving comfort,” *CSEE Journal of Power and Energy Systems*, vol. 6, no. 4, pp. 749–759, 2020, doi: 10.17775/CSEEJPES.2020.02590.

[22] S. Akbari, S. S. Fazel, and S. Jadid, “Optimal operation of a smart railway station based on a multi-energy hub structure considering environmental perspective and regenerative braking utilization,” *Energy Sci Eng*, vol. 9, no. 9, pp. 1614–1631, 2021, doi:10.1002/ese3.937.

[23] I. Şengör, H. C. Kiliçkiran, H. Akdemir, B. Kekezoğlu, O. Erdinç, and J. P. S. Catalão, “Energy Management of a Smart Railway Station Considering Regenerative Braking and Stochastic Behaviour of ESS and PV Generation,” *IEEE Trans Sustain Energy*, vol. 9, no. 3, pp. 1041–1050, 2018, doi:10.1109/TSTE.2017.2759105.

[24] Z. He, C. Wan, and Y. Song, “Frequency Regulation From Electrified Railway,” *IEEE Transactions on Power Systems*, vol. 8950, no. c, pp. 1–18, 2021, doi:10.1109/TPWRS.2021.3119706.

[25] I. M. Saleh *et al.*, “Impact of demand side response on a commercial retail refrigeration system,” *Energies (Basel)*, vol. 11, no. 2, 2018, doi:10.3390/en11020371.

[26] S. Williams, M. Short, and T. Crosbie, “On the use of thermal inertia in building stock to leverage decentralised demand side frequency regulation services,” *Appl Therm Eng*, vol. 133, no. November 2017, pp. 97–106, 2018, doi: 10.1016/j.applthermaleng.2018.01.035.

[27] I. M. Alotaibi, M. A. Abido, and M. Khalid, “Primary Frequency Regulation by Demand Side Response,” *Arab J Sci Eng*, vol. 46, no. 10, pp. 9627–9637, 2021, doi: 10.1007/s13369-021-05440-x.

[28] K. Almaksour *et al.*, “Comparison of dynamic models for a DC railway electrical network including an AC/DC bi-directional power station,” *Math Comput Simul*, vol. 184, pp. 244–266, 2021, doi: 10.1016/j.matcom.2020.05.027.

[29] H. Alnuman, D. Gladwin, and M. Foster, “Electrical modelling of a DC railway system with multiple trains,” *Energies (Basel)*, vol. 11, no. 11, 2018, doi: 10.3390/en11113211.

[30] S. Su, T. Tang, and Y. Wang, “Evaluation of strategies to reducing traction energy consumption of metro systems using an Optimal Train Control Simulation model,” *Energies (Basel)*, vol. 9, no. 2, pp. 1–19, 2016, doi: 10.3390/en9020105.

[31] R. Matthew, F. Flinders, and W. Oghanna, “Locomotive ‘total systems’ simulation using SIMULINK,” *IEE Conference Publication*, no. 405, pp. 202–206, 1995, doi: 10.1049/cp:19950207.

[32] C. S. Chang, A. Khambadkone, and Z. Xu, “Modeling and simulation of DC transit system with VSI-fed induction motor driven train using PSB/MATLAB,” *Proceedings of the International Conference on Power Electronics and Drive Systems*, vol. 2, pp. 881–885, 2001, doi: 10.1109/peds.2001.975436.

[33] F. Du, J. He, L. Yu, M. Li, Z. Bo, and A. Klimek, “Modeling and simulation of metro DC traction system with different motor driven trains,” *Asia-Pacific Power and Energy Engineering Conference, APPEEC*, pp. 5–8, 2010, doi: 10.1109/APPEEC.2010.5448372.

[34] A. Capasso, R. Lamedica, A. Ruvio, M. Ceraolo, and G. Lutzemberger, “Modelling and simulation of electric urban transportation systems with energy storage,” *EEEIC 2016 - International Conference on Environment and Electrical Engineering*, 2016, doi: 10.1109/EEEIC.2016.7555480.

[35] C. Cole, M. Spiryagin, Q. Wu, and Y. Q. Sun, “Modelling, simulation and applications of longitudinal train dynamics,” *Vehicle System Dynamics*, vol. 55, no. 10, pp. 1498–1571, 2017, doi: 10.1080/00423114.2017.1330484.

[36] L. Yang, X. Li, and J. Tu, “Thermal comfort analysis of a high-speed train cabin considering the solar radiation effects,” *Indoor and Built Environment*, vol. 29, no. 8, pp. 1101–1117, 2020, doi: 10.1177/1420326X19876082.

[37] S. Istomin and A. Shtraukhman, “Simulation model of the heating and air conditioning system of dc electric trains,” in *E3S Web of Conferences*, 2019, vol. 135, p. 9, doi: 10.1051/e3sconf/201913502018.

[38] R. Mastrullo, A. W. Mauro, and C. Vellucci, “Refrigerant Alternatives for High Speed Train A/C Systems: Energy Savings and Environmental Emissions Evaluation under Variable Ambient Conditions,” *Energy Procedia*, vol. 101, no. September, pp. 280–287, 2016, doi: 10.1016/j.egypro.2016.11.036.

[39] W. Pan, S. C. Dhulipala, and A. S. Bretas, “A distributed approach for DG integration and power quality management in railway power systems,” *Conference Proceedings - 2017 17th IEEE International Conference*

on Environment and Electrical Engineering and 2017 1st IEEE Industrial and Commercial Power Systems Europe, EEEIC / I and CPS Europe 2017, 2017, doi: 10.1109/EEEIC.2017.7977714.

[40] N. Li, L. Yang, X. Li, X. Li, J. Tu, and S. C. P. Cheung, "Multi-objective optimization for designing of high-speed train cabin ventilation system using particle swarm optimization and multi-fidelity Kriging," *Build Environ*, vol. 155, no. March, pp. 161–174, 2019, doi: 10.1016/j.buildenv.2019.03.021.

[41] J. A. Thompson, G. G. Maidment, and J. F. Missenden, "Modelling low-energy cooling strategies for underground railways," *Appl Energy*, vol. 83, no. 10, pp. 1152–1162, 2006, doi: 10.1016/j.apenergy.2005.12.001.

[42] K. Jenkins, M. Gilbey, J. Hall, V. Glenis, and C. Kilsby, "Implications of climate change for thermal discomfort on underground railways," *Transp Res D Transp Environ*, vol. 30, pp. 1–9, 2014, doi: 10.1016/j.trd.2014.05.002.

[43] R. N. Hofstädter, T. Zero, C. Dullinger, G. Richter, and M. Kozek, "Heat capacity and heat transfer coefficient estimation for a dynamic thermal model of rail vehicles," *Math Comput Model Dyn Syst*, vol. 23, no. 5, pp. 439–452, 2017, doi: 10.1080/13873954.2016.1263670.

[44] P. H. Hsi, S. L. Chen, and R. J. Li, "Simulating on-line dynamic voltages of multiple trains under real operating conditions for AC railways," *IEEE Transactions on Power Systems*, vol. 14, no. 2, pp. 452–459, 1999, doi: 10.1109/59.761865.

[45] P. Kundur, *Power System Stability and Control*, EPRI. Palo Alto, California: McGrawHill, 1994.

[46] D. Ochoa and S. Martinez, "Proposals for enhancing frequency control in weak and isolated power systems: Application to the wind-diesel power system of San Cristobal Island-Ecuador," *Energies (Basel)*, vol. 11, no. 4, p. 25, 2018, doi: 10.3390/en11040910.

[47] Secretaría Nacional de Energía (SNE), "Guía de Construcción Sostenible para el Ahorro de Energía en Edificaciones y medidas para el uso racional y eficiente de la energía, para la construcción de nuevas edificaciones en la República de Panamá," no. Nov. Gaceta oficial, Panama City, Republic of Panama, pp. 1–57, 2016.

[48] Samsuddin, R. Rahim, B. Hamzah, and R. Mulyadi, "Proposed model of neutral temperature equation for adaptive thermal comfort in student flats units in the tropics," *Civil Engineering and Architecture*, vol. 9, no. 2, pp. 477–492, 2021, doi: 10.13189/cea.2021.090220.

[49] N. Clausen, T. Cronin, and W. Jowittt, "Planning and Development of Wind Farms: Environmental impact and grid connection Wind Energy," Lyngby, Denmark, 2013.

[50] J. Araúz, D. Mora, and M. Chen Austin, "Assessment of Different Envelope Configurations via Optimization Analysis and Thermal Performance Indicators: A Case Study in a Tropical Climate," *Sustainability (Switzerland)*, vol. 14, no. 4, p. 20, doi: 10.3390/su14042013.

[51] Red Eléctrica de España, "Establecimiento de la reserva para la regulación frecuencia-potencia," *Boletín Oficial del Estado N°173*, 2006. https://www.ree.es/sites/default/files/01_ACTIVIDADES/Documentos/ProcedimientosOperacion/RES_PO_1.5.pdf (accessed Feb. 15, 2022).

[52] R. Quint and D. Ramasubramanian, "Impacts of droop and deadband on generator performance and frequency control," *IEEE Power and Energy Society General Meeting*, vol. January, pp. 1–5, 2018, doi: 10.1109/PESGM.2017.8274729.